J Gastroenterol
DOI 10.1007/s00535-015-1054-3

The Japanese Society of Gastroenterology

ORIGINAL ARTICLE—LIVER, PANCREAS, AND BILIARY TRACT

Migration of splenic lymphocytes promotes liver fibrosis through modification of T helper cytokine balance in mice

Kazutaka Tanabe · Kojiro Taura · Yukinori Koyama · Gen Yamamoto · Takahiro Nishio · Yukihiro Okuda · Kojiro Nakamura · Kan Toriguchi · Kenji Takemoto · Kenya Yamanaka · Keiko Iwaisako · Satoru Seo · Masataka Asagiri · Etsuro Hatano · Shinji Uemoto

Received: 13 July 2014 / Accepted: 7 February 2015

Abstract
Background Sustained liver injury causes liver fibrosis and eventually cirrhosis. Understanding the pathophysiological mechanisms of liver fibrosis and interventions in the fibrotic process is crucial for improving the prognosis of patients with chronic liver diseases. Although studies have shown that splenectomy suppresses liver fibrosis, the mechanism by which this occurs is poorly understood. The present study focuses on the immunological functions of the spleen to investigate its role in liver fibrosis.
Methods BALB/c and severe combined immunodeficiency (SCID) mice underwent splenectomies or sham operations prior to induction of liver fibrosis with carbon tetrachloride or thioacetamide.
Results Sirius red staining and hydroxyproline assays showed that splenectomy suppressed liver fibrogenesis in BALB/c mice. Reverse transcription PCR analysis of T helper type 1 (Th1) and T helper type 2 (Th2) cytokines demonstrated that splenectomy shifted the Th1/Th2 balance in the liver towards Th1 dominance. In SCID mice, the inhibitory effect on liver fibrosis was abrogated. The number of $CD4^+$ T helper lymphocytes in the spleen decreased after liver injury. Green fluorescent protein positive (GFP^+) splenocytes were transplanted into the spleens of syngeneic wild-type mice to trace their destination after fibrosis induction. GFP^+CD4^+ lymphocytes appeared in the liver after induction of fibrosis, and flow cytometry revealed the vast majority of them were Th2 lymphocytes. Transfer of splenocytes via the portal vein into syngeneic splenectomized mice cancelled the suppressive effect of splenectomy on liver fibrosis.
Conclusions The present study demonstrated that Th2-dominant splenic lymphocytes migrate into the liver and promote liver fibrosis by shifting the cytokine balance towards Th2 dominance. Splenectomy suppresses the progression of fibrosis at least partly by restoring the Th1/Th2 balance.

Keywords Splenectomy · Liver fibrosis · T helper lymphocyte

Abbreviations

BDL	Bile duct ligation
GFP	Green fluorescent protein
IL	Interleukin
PBS	Phosphate-buffered saline
qRT-PCR	Quantitative reverse transcription PCR
SCID	Severe combined immunodeficiency
α-SMA	α-Smooth muscle actin

Electronic supplementary material The online version of this article (doi:10.1007/s00535-015-1054-3) contains supplementary material, which is available to authorized users.

K. Tanabe · K. Taura (✉) · Y. Koyama · G. Yamamoto · T. Nishio · Y. Okuda · K. Nakamura · K. Toriguchi · K. Takemoto · K. Yamanaka · S. Seo · E. Hatano · S. Uemoto
Department of Surgery, Graduate School of Medicine, Kyoto University, 54 Kawahara-cho, Shogoin, Sakyo-ku, Kyoto 6068507, Japan
e-mail: ktaura@kuhp.kyoto-u.ac.jp

K. Tanabe
e-mail: tanabe75@kuhp.kyoto-u.ac.jp

K. Iwaisako
Department of Target Therapy Oncology, Graduate School of Medicine, Kyoto University, 54 Kawaharacho, Shogoin, Sakyo-ku, Kyoto 606-8507, Japan

M. Asagiri
Innovation Center for Immunoregulation and Therapeutics, Graduate School of Medicine, Kyoto University, Yoshida Konoe, Sakyo-ku, Kyoto 606-8501, Japan

Published online: 28 February 2015

TAA	Thioacetamide
Th1	T helper type 1
Th2	T helper type 2

Introduction

Sustained liver injury results in liver fibrosis regardless of the cause. Hepatic fibrosis is characterized by a progressive accumulation of fibrillar extracellular matrix proteins in the liver that distorts the hepatic architecture and may eventually result in liver cirrhosis [1]. Since the progression of liver fibrosis is directly associated with complications in chronic liver diseases, understanding the pathophysiological mechanisms of liver fibrosis and intervention in the fibrotic process is crucial for improving the prognosis of patients with chronic liver diseases. Hypersplenism is a major complication in patients with advanced liver fibrosis. For those patients, splenectomy is beneficial and often indicated as it increases the platelet count and makes antiviral therapy or invasive treatment feasible [2]. Moreover, clinical observations have revealed that splenectomy not only increases the platelet count, but also improves liver function [3, 4]. In addition, some experimental studies have shown that splenectomy suppresses the progression of liver fibrosis. The underlying mechanisms are largely unknown, although a few studies have proposed explanations for this phenomenon [5–7].

The spleen plays important roles in the immune system. Specifically, B cells and plasma cells mature in the spleen, and have key functions in humoral immunity. Moreover, T cells and the cytokines they produce play important roles in modifying the maturation process of these lymphocytes. Importantly, the immune system can affect the progression of liver fibrosis; for instance, strain-specific differences in murine hepatic fibrotic responses are mediated by divergent T helper cytokine responses [8]. In addition, immunosuppressants differently modulate hepatic fibrotic responses in mice and humans [9, 10]. These observations have led us to the hypothesis that the spleen modulates liver fibrosis through its immunological functions. The present study aimed to investigate the role of the spleen in liver fibrosis, with particular focus on its immunological functions.

Materials and methods

Animals

BALB/c, C57BL/6, severe combined immunodeficiency (SCID), and C57BL/6-Tg(CAG-EGFP)C14-Y01-FM131Osb ("green mice") male mice were purchased at 10 weeks of age from Japan SLC (Shizuoka, Japan) and CLEA Japan (Tokyo, Japan). After acclimation for 7 days, the mice were divided into sham-operation and splenectomy groups. Splenectomies were performed under pentobarbital anaesthesia (50 mg/kg) as previously described [5]. Splenic arteries and veins were ligated twice with 6-0 nylon sutures with a minimal incision on the upper abdominal midline. Sham-operation mice underwent a laparotomy without splenectomy. The protocol for animal handling was reviewed and approved by the Animal Care and Use Committee of Kyoto University.

Experimental liver fibrosis models

Liver fibrosis was induced by repetitive injections of carbon tetrachloride (CCl_4) or thioacetamide (TAA). In the CCl_4-induced liver fibrosis model, each mouse was subjected to intraperitoneal injections of CCl_4 (0.5 μL/g body weight; 1:4 dilution with corn oil) or corn oil as a control twice a week for 6 weeks [11]. Livers were harvested 7 days after the last injection. TAA-induced liver fibrosis was induced by intraperitoneal injections with escalating doses of TAA or normal saline as a control three times a week for 6 weeks (first dose, 100 mg/kg, weeks 1–2, 200 mg/kg; weeks 3–4, 300 mg/kg; weeks 4–6, 400 mg/kg), as previously described [12]. Livers were harvested 3 days after the last injection. Bile duct ligation (BDL) was performed by surgical ligation of the common bile duct, as previously described [13]. The common bile duct was ligated three times with 6-0 nylon sutures under pentobarbital anaesthesia (50 mg/kg). Sham-operation mice underwent laparotomy without ligation of the common bile duct. Mice were killed for analysis at 10 days and 3 weeks after the operation.

Sirius red staining

Formalin-fixed specimens were embedded in paraffin, sliced with a thickness of 4 μm, and mounted on silanized glass slides. Sirius red staining was performed as previously described [13]. Ten nonoverlapping fields per mouse at a final magnification of ×100 were randomly selected and photographed. The Sirius red positive area was quantified using an image analysis software package (Image J; National Institutes of Health).

Immunofluorescence staining

The specimens were fixed in 4 % paraformaldehyde, embedded in OCT compound, and sliced with a thickness of 5 μm. Antigen retrieval was performed by incubation in citric acid buffer at 90 °C, for 20 min. After blocking, the sections were incubated with a primary antibody against α-smooth muscle actin (α-SMA; ab5694; Abcam,

Cambridge, UK), CD4 (IH95-0042; eBioscience, San Diego, CA, USA), CD45RC (ab3135; Abcam), or green fluorescent protein (GFP; A1122; Invitrogen, Carlsbad, CA, USA) at 1:100 dilution overnight at 4 °C, and were then incubated with a corresponding secondary antibody at room temperature for 1 h. The CD4-positive area was evaluated as a percentage using Image J.

Hydroxyproline content measurement

Liver tissues were homogenized in ice-cold distilled water (1 mL). Subsequently, 125 μL of 50 % trichloroacetic acid was added, and the homogenates were incubated on ice for 30 min. The precipitated pellets were hydrolysed for 24 h at 110 °C in 6 N HCl. After hydrolysis, the samples were

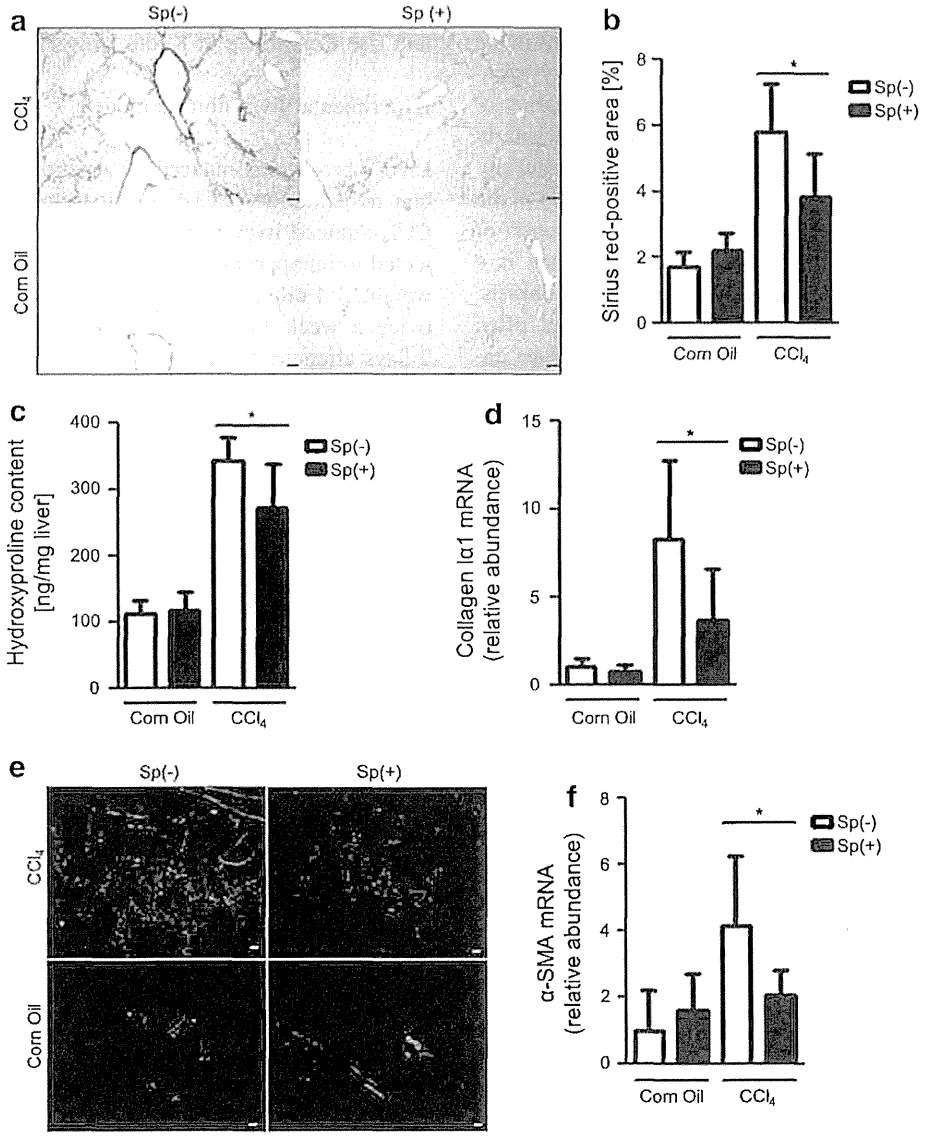

Fig. 1 Splenectomy suppresses the progression of liver fibrosis in a CCl_4-induced liver injury mouse model. BALB/c mice were divided into sham-operation and splenectomy groups and received injections of CCl_4 ($n = 7$ mice per group) or corn oil ($n = 6$ mice per group). **a** Liver fibrosis was evaluated by Sirius red staining. Original magnification ×40. **b** The Sirius red positive area was quantified as a percentage using Image J. **c** Collagen deposition was quantified by measuring the hydroxyproline content in the liver. **d** Quantitative reverse transcription PCR (qRT-PCR) was performed to measure messenger RNA (*mRNA*) expression levels of *Col1a1* (which encodes type I collagen α_1). *Gapdh* (which encodes glyceraldehyde 3-phosphate dehydrogenase) was used as an internal control. **e** Activation of hepatic stellate cells was evaluated by immunofluorescence staining for α-smooth muscle actin (*α-SMA*; which is encoded by *Acta2*). Original magnification ×100. **f** Hepatic expression levels of *Acta2* mRNA were measured using qRT-PCR. *Gapdh* was used as an internal control. The mean ± the standard deviation is shown. *Asterisks* indicate statistically significant differences ($P < 0.05$) determined by the Mann–Whitney *U* test. *Sp(-)* sham-operation group, *Sp(+)* splenectomy group

filtered, neutralized with 10 N NaOH, and oxidized with chloramine-T (Sigma-Aldrich, St Louis, MO, USA) for 25 min at room temperature. The reaction mixture was incubated in Ehrich's perchloric acid solution at 65 °C for 20 min and then cooled to room temperature. Sample absorbance was measured at 560 nm in duplicate. Purified hydroxyproline (Sigma-Aldrich) was used as a standard. The hydroxyproline content was expressed as nanograms of hydroxyproline per milligram of liver.

Quantitative reverse transcription PCR analysis

Total RNA was extracted from liver samples using TRIzol (Invitrogen, Tokyo, Japan) and RNeasy Mini kits with on-column DNA digestion (Qiagen, Tokyo, Japan). Total RNA was reverse transcribed to complementary DNA using an Omniscript reverse transcription kit (Qiagen, Valencia, CA, USA). We performed quantitative reverse transcription PCR (qRT-PCR) with gene-specific PCR primers (Table S1) and SYBR Green I master reaction mix using a LightCycler 480 II instrument (Roche Diagnostics, Basel, Switzerland). The relative abundance of the target genes was determined by comparison with a standard curve and was normalized to the abundance of *Gapdh* as an internal control using the LightCycler 480 software (version 1.5).

Isolation of hepatic lymphoid cells

Hepatic lymphoid cells were isolated from murine livers by a method described previously [13, 14]. Livers were minced into small fragments and washed free of blood in cold phosphate-buffered saline (PBS). Fragments were passed through a 100-μm steel mesh. The cell suspension was filtered through a nylon mesh (BD Falcon cell strainer; BD Biosciences) to remove tissue debris. Filtered cells were centrifuged at 50*g* for 1 min to remove the hepatocyte fraction. The remaining nonparenchymal cell fraction was collected, washed, and resuspended in PBS. Leukocytes were isolated by density-gradient centrifugation (Histopaque-1077; Sigma-Aldrich). Cell viability was assessed by trypan blue staining.

Isolation of lymphocytes from spleen

Spleens were minced through a nylon mesh (BD Falcon cell strainer; BD Biosciences) to obtain single-cell suspensions in PBS as previously described [15]. Erythrocytes were lysed by incubation in lysis buffer (00-4333-57; eBioscience, San Diego, CA, USA) for 4 min at room temperature. Following these procedures, lymphocytes were washed twice in PBS by centrifugation at 300*g* at 4 °C and were resuspended in PBS.

Fig. 2 Splenectomy modifies the T helper type 1 (*Th1*)/T helper type 1 (*Th2*) balance in the liver in a CCl_4-induced liver injury model. Quantitative reverse transcription PCR (qRT-PCR) was performed to measure hepatic messenger RNA (*mRNA*) expression levels of **a** *Ifng*, *Il2*, and *Il12a*/*Il12b* (which encode Th1 cytokines) and **b** *Il4* and *Il13* (which encode Th2 cytokines). *Gapdh* was used as an internal control. **c** The ratio of the mRNA expression levels of *Ifng* (Th1) to *Il4* (Th2) in each mouse was compared between the CCl_4 sham-operation group and the CCl_4 splenectomy group. **d** The mRNA expression levels of *Tgfb1* (which encodes a potent profibrogenic cytokine) were measured by qRT-PCR. **e** Intrahepatic lymphocytes were isolated from CCl_4 splenectomy and sham-operation mice and were subjected to flow-cytometric analysis for expression of CD4 and CD45RC. The statistical result found in at least seven mice is shown. **f** Double immunofluorescence staining for CD45RC (*green*) and CD4 (*red*). The number of $CD4^+$ cells and $CD45RC^+CD4^+$ cells were counted under a magnification of ×100, and the proportion of $CD45RC^+CD4^+$ cells among $CD4^+$ cells in the liver is shown. ($n = 7$ for CCl_4 groups, $n = 6$ for control groups). The mean ± the standard deviation is shown. $^*P < 0.05$, $^{**}P < 0.01$, $^{***}P < 0.001$, *DAPI* 4′,6-diamidino-2-phenylindole, *IFN* interferon, *IL* interleukin, *ns* not significant ($P > 0.05$), *Sp(-)* sham-operation group, *Sp(+)* splenectomy group, *TGF* transforming growth factor

Flow-cytometric analysis

Hepatic lymphoid cell isolation from liver tissues and staining for flow cytometry were performed as described in [14]. In brief, lymphoid cells were stained with anti-CD4 (BD Pharmingen 553051; BD Biosciences, San Diego, CA, USA) and anti-CD45RC (BD Pharmingen 557357; BD Biosciences San Diego, CA, USA) mouse antibodies labelled with allophycocyanin and phycoerythrin, respectively. Three-colour flow-cytometric analyses were performed using a BD Accuri C6 flow cytometer (BD Biosciences, San Jose, CA, USA).

Statistical analysis

Quantitative data are expressed as the mean ± the standard deviation. For statistical analysis, we used the Mann–Whitney *U* test. *P* values less than 0.05 were regarded as statistically significant.

Results

Splenectomy suppresses progression of liver fibrosis induced by CCl_4 and TAA in mice

Liver fibrosis was induced by repetitive administration of CCl_4 for 6 weeks, and hepatic collagen deposition was evaluated by Sirius red staining of the liver sections. In the corn oil control groups, Sirius red staining demonstrated no fibrous regions, except in the portal areas. Collagen deposition was observed in the livers of mice that received CCl_4 for 6 weeks. The area of fibrous changes in the CCl_4

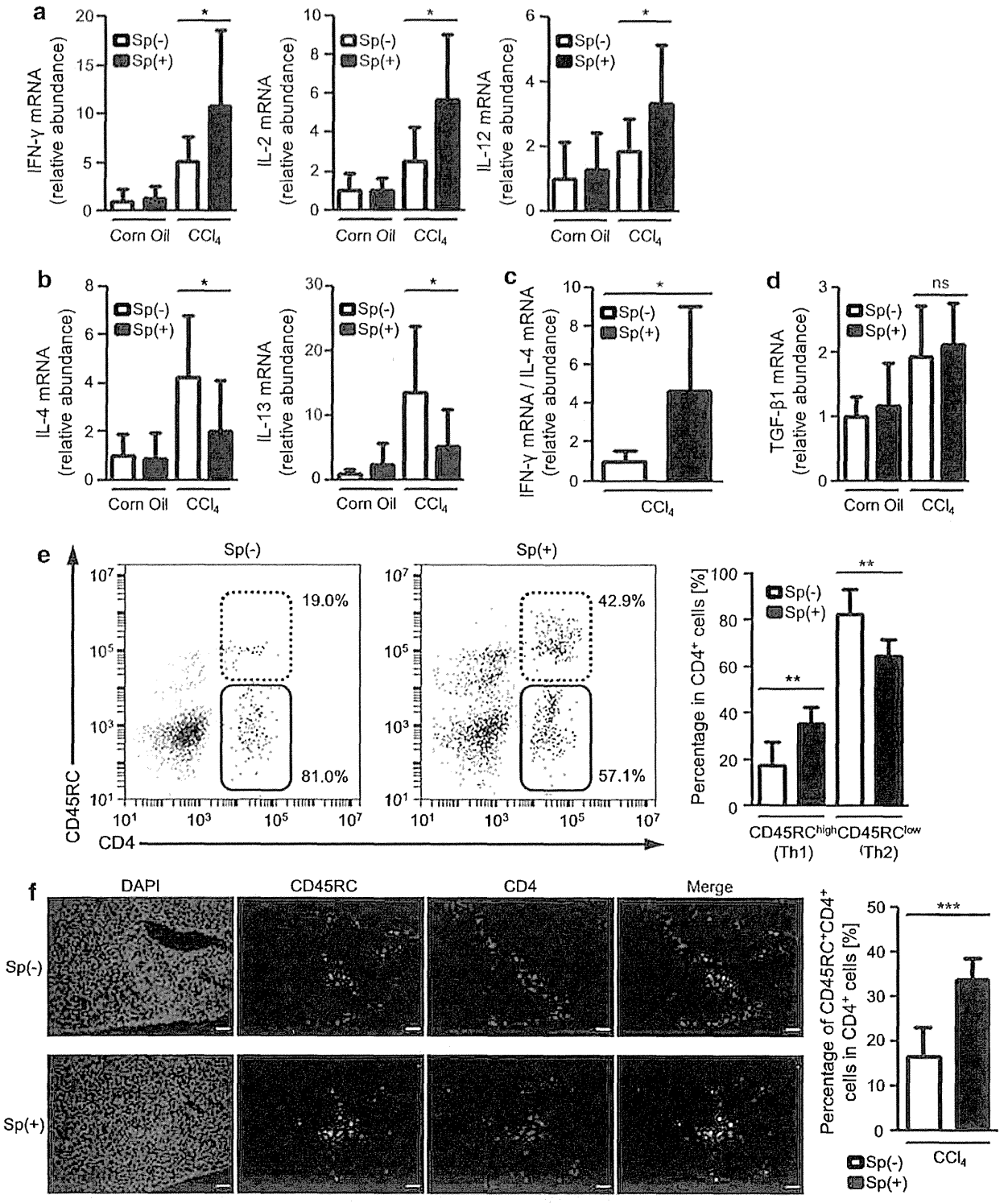

splenectomy group was markedly attenuated compared with that of the CCl_4 sham-operation group (Fig. 1a). The Sirius red positive area quantified by Image J was significantly reduced in the CCl_4 splenectomy group compared with the CCl_4 sham-operation group (3.82 ± 1.29 % vs 5.79 ± 1.43 %; $P = 0.018$; Fig. 1b). The hepatic content of

hydroxyproline, a biochemical marker of collagen accumulation, was elevated to 344 ± 34.2 ng/mg liver in the CCl_4 sham-operation group (Fig. 1c). Comparatively, it was reduced to 274 ± 64.7 ng/mg liver in the CCl_4 splenectomy group, resulting in a statistically significant difference between the two groups ($P = 0.018$). Hepatic expression of *Col1a1* (which encodes type I collagen α_1) evaluated by qRT-PCR was increased by 8.1-fold in the CCl_4 sham-operation group as compared with the corn oil group (Fig. 1d). By comparison, *Col1a1* expression was suppressed by 4.5-fold in the CCl_4 splenectomy group ($P = 0.026$). Activation of hepatic stellate cells was evaluated by immunostaining for α-SMA. Immunostaining for α-SMA in the CCl_4 sham-operation group demonstrated a significant increase in the number of α-SMA-positive cells. The number of α-SMA-positive cells in the CCl_4 splenectomy group was lower than in the CCl_4 sham-operation group (Fig. 1e). Similarly, hepatic expression of *Acta2* (which encodes α-SMA) was significantly lower in the CCl_4 splenectomy group than in the CCl_4 sham-operation group ($P = 0.038$; Fig. 1f).

The effect of splenectomy on liver fibrosis was also investigated using the TAA-induced liver injury model (Fig. S1). Sirius red staining demonstrated that collagen deposition in the TAA splenectomy group was significantly decreased compared with that in the TAA sham-operation group. The ratio of the fibrous area in the TAA splenectomy group was reduced compared with that in the TAA sham-operation group (6.62 ± 1.65 % vs 8.84 ± 0.82 %; $P = 0.007$). The hydroxyproline content was elevated to 277 ± 59.7 ng/mg liver in the TAA sham-operation group and was reduced to 221 ± 24.3 ng/mg liver in the TAA splenectomy group ($P = 0.038$). Hepatic expression of *Col1a1* was suppressed in the TAA splenectomy group compared with the TAA sham-operation group ($P = 0.038$). Immunostaining for α-SMA demonstrated that the number of α-SMA-positive cells in the TAA splenectomy group was lower than that in the TAA sham-operation group. Hepatic expression of *Acta2* was also suppressed in the TAA splenectomy group compared with the TAA sham-operation group ($P = 0.026$).

These results indicate that splenectomy suppressed collagen synthesis in the liver and alleviated liver fibrosis in the CCl_4-induced and TAA-induced liver injury models.

We also investigated the effect of splenectomy in the BDL-induced liver injury model (Fig. S2). Sirius red staining demonstrated remarkable fibrotic changes in the BDL-induced liver injury model. In contrast to the toxin-induced liver fibrosis model, the fibrotic area was not different between the BDL sham-operation group and the BDL splenectomy group at both 10 days and 3 weeks after BDL (10 days, 7.97 ± 1.82 % vs 7.47 ± 2.28 %, $P = 0.779$; 3 weeks, 9.51 ± 1.67 % vs 8.25 ± 2.23 %, $P = 0.456$). The hydroxyproline content was also similar between the two groups (10 days, 181 ± 32.9 ng/mg liver vs 165 ± 42.8 ng/mg liver, $P = 0.463$; 3 weeks, 418 ± 83.2 ng/mg liver vs 451 ± 200 ng/mg liver, $P = 0.209$). In addition, hepatic expression of *Col1a1* and *Acta2* was comparable between the two groups (10 days, $P = 0.902$ and $P = 0.165$, respectively; 3 weeks, $P = 0.902$ and $P = 0.383$; respectively).

Splenectomy modifies the T helper type 1/T helper type 2 balance in toxin-induced liver fibrosis models

We analysed the effect of splenectomy on the inhibition of fibrotic responses induced in toxin-induced liver injury models, especially focusing on the T helper type 1 (Th1)/T helper type 2 (Th2) balance. Liver fibrosis was induced by repetitive administration of CCl_4 for 6 weeks, and livers were harvested 7 days after the last injection. Expression of *Ifng* mRNA (*Ifng* encodes interferon-γ, a typical Th1 cytokine) was increased by 5.0-fold in the CCl_4 sham-operation group in comparison with the corn oil control group. Expression of *Ifng* mRNA was further enhanced by 8.2-fold in the CCl_4 splenectomy group ($P = 0.038$; Fig. 2a). Similarly, expression of *Il2* [which encodes interleukin (IL)-2] and *Il12a*/*Il12b* (which encode IL-12) mRNA was increased by 2.6-fold and 1.8-fold in the CCl_4 sham-operation group, and this increase was further enhanced by 5.4-fold and 2.6-fold, respectively, in the CCl_4 splenectomy group (*Il2*, $P = 0.038$; *Il12a*/*Il12b*, $P = 0.038$; Fig. 2a). In the CCl_4 sham-operation group in comparison with the corn oil group, expression of *Il4* mRNA (*Il4* encodes IL-4, a representative Th2 cytokine) was increased by 4.2-fold. In contrast to the Th1 cytokines, *Il4* mRNA expression was suppressed by 2.4-fold in the CCl_4 splenectomy group ($P = 0.038$; Fig. 2b). Similarly, *Il13* mRNA expression was increased by 13-fold in the CCl_4 sham-operation group, and this increase was inhibited by 2.2-fold after splenectomy ($P = 0.038$; Fig. 2b). The ratio of *Ifng* (Th1) to *Il4* (Th2) mRNA expression in each mouse was increased by 4.7-fold in the CCl_4 splenectomy group compared with the CCl_4 sham-operation group ($P = 0.038$; Fig. 2c). The expression levels of *Tgfb1* (which encodes transforming growth factor β_1, one of the most potent profibrogenic cytokines) did not differ between the CCl_4 splenectomy and CCl_4 sham-operation groups [16] ($P = 0.383$; Fig. 2d). We also evaluated Th1 and Th2 cytokine expression from lymphocytes isolated from livers (Fig. S3). Similarly to the results obtained from the whole liver tissue, Th1 cytokines were upregulated whereas Th2 cytokines were downregulated in the CCl_4 splenectomy group in comparison with the CCl_4 sham-operation group. The ratio of *Ifng* to *Il4* mRNA expression was increased by 2.5-fold in the CCl_4 splenectomy group compared with the CCl_4 sham-operation group ($P = 0.0082$). The Th1/Th2

balance in the liver was also evaluated, on the basis of different CD45RC expression profiles between Th1 and Th2 lymphocytes [17, 18]. Flow-cytometric analysis revealed a significant increase in the proportion of Th1 ($CD45RC^{high}CD4^{+}$) lymphocytes among $CD4^{+}$ lymphocytes in the CCl_4 splenectomy group compared with the CCl_4 sham-operation group (35.6 ± 7.2 % vs 17.3 ± 10.2 %; Fig. 2e). Double immunostaining for CD45RC and CD4 in the CCl_4 splenectomy group demonstrated a significant increase in the number of $CD45RC^{+}CD4^{+}$ cells (Th1) after CCl_4 treatment compared with the CCl_4 sham-operation group. The ratio of $CD45RC^{+}CD4^{+}$ cells to $CD4^{+}$ cells was 33.8 ± 4.63 % in the CCl_4 splenectomy group, whereas it was 16.7 ± 6.50 % in the CCl_4 sham-operation group ($P = 0.0003$; Fig. 2f).

We also investigated the change in the liver Th1/Th2 balance resulting from splenectomy in the TAA-induced liver injury model (Fig. S4). The expression levels of *Ifng*, *Il2*, and *Il12a/Il12b* mRNA were increased by 3.8-, 3.0-, and 2.8-fold, respectively, in the TAA sham-operation group in comparison with the control saline group. The expression of *Ifng*, *Il2*, and *Il12a/Il12b* mRNA was enhanced by 5.5-, 7.5-, and 5.3-fold, respectively, in the TAA splenectomy group (*Ifng*, $P = 0.038$; *Il2*, $P = 0.038$; *Il12a/Il12b*, $P = 0.038$). In contrast, the expression levels

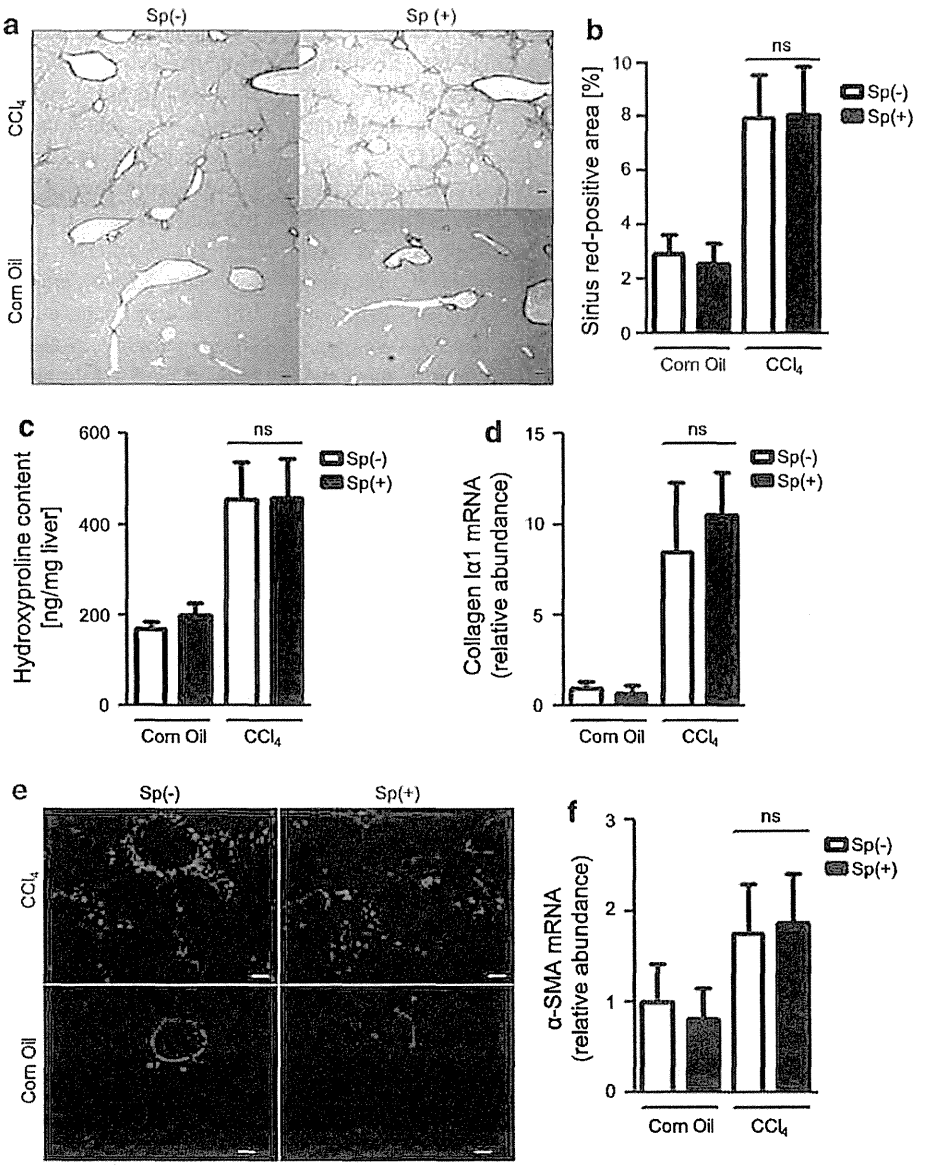

Fig. 3 Suppressive effect of splenectomy on liver fibrosis is abrogated in immunodeficient severe combined immunodeficiency (SCID) mice. SCID mice were divided into sham-operation and splenectomy groups, and received injections of CCl_4 ($n = 7$ mice per group) or corn oil ($n = 6$ mice per group). **a** Liver fibrosis was evaluated by Sirius red staining. Original magnification ×40. **b** The Sirius red positive area was quantified as a percentage using Image J. **c** Collagen deposition was quantified by measuring the hydroxyproline content in the liver. **d** Quantitative reverse transcription PCR (qRT-PCR) was performed to measure messenger RNA (*mRNA*) expression levels of *Col1a1*. *Gapdh* was used as an internal control. **e** Activation of hepatic stellate cells was evaluated by immunofluorescence staining for α-smooth muscle actin (*α-SMA*). Original magnification ×100. **f** Hepatic expression levels of *Acta2* mRNA were measured by qRT-PCR. *Gapdh* was used as an internal control. The mean ± the standard deviation is shown. *ns* not significant, *Sp(-)* sham-operation group, *Sp(+)* splenectomy group

of *Il4* and *Il13* mRNA were increased by 5.2- and 7.7-fold in the TAA sham-operation group compared with the saline group. Moreover, their expression levels were inhibited by 4.2- and 3.3-fold, respectively, in the TAA splenectomy group (*Il4*, $P = 0.038$; *Il13*, $P = 0.026$). The ratio of *Ifng* to *Il4* mRNA expression was increased by 3.0-fold in the TAA splenectomy group compared with the TAA sham-operation group ($P = 0.007$). The expression level of *Tgfb1* was not altered by splenectomy in the TAA-induced liver injury model ($P = 0.805$). The proportion of $CD45RC^{high}CD4^+$ lymphocytes among $CD4^+$ lymphocytes in the TAA splenectomy group measured by flow cytometry was increased compared with that in the TAA sham-operation group (39.8 ± 2.9 % vs 21.2 ± 7.1 %). The ratio of $CD45RC^+CD4^+$ cells to $CD4^+$ cells was also increased in the TAA splenectomy group compared with the TAA sham-operation group, as demonstrated by immunostaining (35.2 ± 4.84 % vs 19.6 ± 3.58 %; $P = 0.0002$). Taken together, these results showed that splenectomy shifted the Th1/Th2 balance in the liver towards Th1 dominance in the toxin-induced liver fibrosis models.

In the BDL-induced liver injury model, there was no statistical difference in the expression levels of *Ifng* and *Il4* mRNA between splenectomy and sham-operation groups at both 10 days and 3 weeks after BDL (Fig. S5).

Effect of splenectomy is abrogated in immunodeficient SCID mice

Immunodeficient SCID mice were used to determine if immunological mechanisms were involved in the effect of splenectomy on liver fibrosis observed in wild-type mice. Although liver fibrosis was similarly induced with CCl_4 in SCID mice as in wild-type mice, the inhibitory effect of splenectomy on liver fibrosis was not observed in SCID mice (Fig. 3a). In addition, the fibrotic area did not differ between CCl_4 splenectomy and sham-operation groups (8.12 ± 1.71 % vs 7.97 ± 1.57 %, $P = 0.902$; Fig. 3b). The hepatic hydroxyproline content was similarly elevated in the CCl_4 splenectomy and sham-operation groups (457 ± 92.8 ng/mg liver vs 454 ± 81.4 ng/mg liver, $P = 0.902$; Fig. 3c). The hepatic expression level of *Col1a1* was not affected by splenectomy ($P = 0.165$; Fig. 3d). Furthermore, splenectomy had no effect on hepatic expression of α-SMA, as demonstrated by immunostaining (Fig. 3e) and qRT-PCR ($P = 0.535$; Fig. 3f).

Next, we evaluated the influence of splenectomy in the immunodeficient SCID mice on cytokine expression in our CCl_4-induced liver fibrosis model. As expected, the expression levels of *Ifng* and *Il4* mRNA were not influenced by splenectomy in SCID mice (Fig. 4a, b). The ratio of *Ifng* to *Il4* mRNA in each SCID mouse was comparable

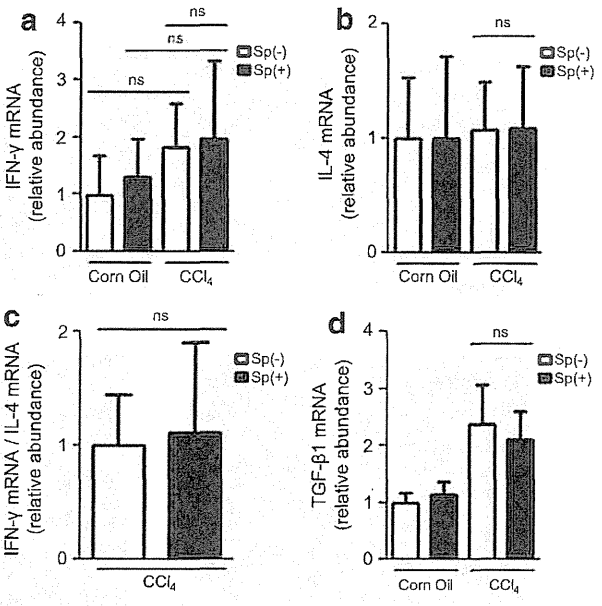

Fig. 4 Hepatic T helper type 1 (Th1)/T helper type 2 (Th2) cytokine expression levels in a CCl_4-induced liver injury model are not modified by splenectomy in immunodeficient severe combined immunodeficiency mice. Quantitative reverse transcription PCR (qRT-PCR) was performed to measure messenger RNA (*mRNA*) expression of *Ifng* (Th1) (**a**) and *Il4* (Th2) (**b**). *Gapdh* was used as an internal control. **c** The ratios of the mRNA expression levels of *Ifng* (Th1) to *Il4* (Th2) in each mouse were compared between the CCl_4 splenectomy and CCl_4 sham-operation groups. **d** The mRNA expression levels of *Tgfb1* (which encodes a potent profibrogenic cytokine) were measured by qRT-PCR. ($n = 7$ for CCl_4 groups, $n = 6$ for control groups). The mean ± the standard deviation is shown. *IFN* interferon, *IL* interleukin, *ns* not significant, *Sp(-)* sham-operation group, *Sp(+)* splenectomy group, *TGF* transforming growth factor

between the CCl_4 splenectomy and sham-operation groups ($P = 0.902$; Fig. 4c). *Tgfb1* mRNA expression levels showed no differences between the CCl_4 splenectomy and sham-operation groups ($P = 0.383$; Fig. 4d).

Number of $CD4^+$ cells in spleen is reduced in toxin-induced liver fibrosis models

Pathophysiological changes in the spleen of toxin-induced liver fibrosis model mice were evaluated to elucidate the mechanisms by which splenectomy suppressed liver fibrosis and modified the Th1/Th2 balance in the liver. Histological examination of spleens by haematoxylin and eosin staining revealed no structural changes between the control group and toxin-induced liver injury groups (Fig. 5a). In the CCl_4-induced liver injury model, we evaluated the serial $CD4^+$ cell counts in the spleen. Immunostaining for the T helper lymphocyte marker CD4 demonstrated a time-dependent decrease in $CD4^+$ cell numbers (Fig. 5b). The CD4-positive area was 8.43 ± 0.82 % before CCl_4 treatment, and it was

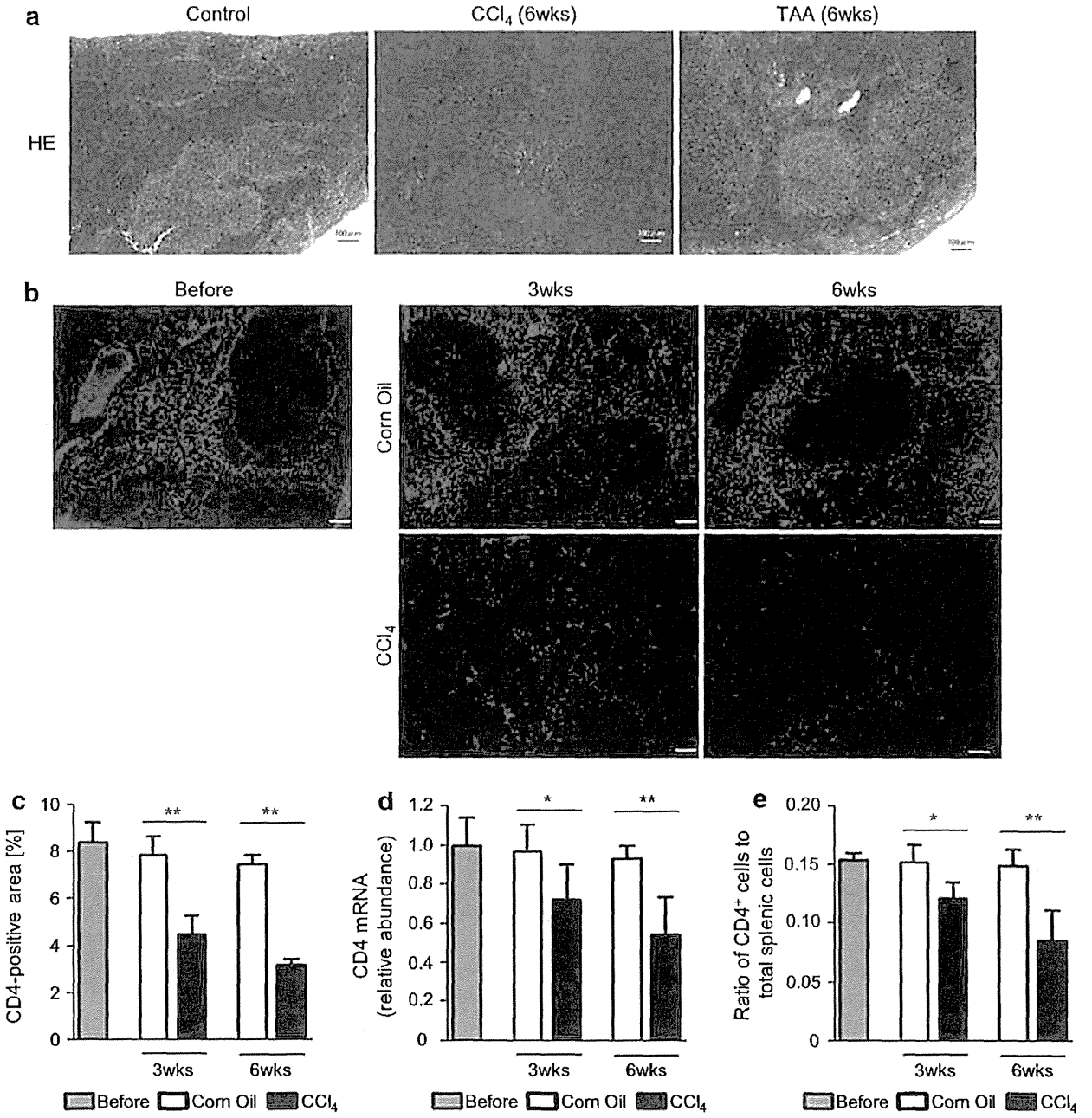

Fig. 5 The number of $CD4^+$ T helper lymphocytes in spleen decreases time-dependently in response to liver injuries. Liver fibrosis was induced by injection of CCl_4 or thioacetamide (*TAA*) as described in "Materials and methods". **a** Haematoxylin and eosin (*HE*) staining of the spleen. Original magnification ×40. **b** The expression of CD4, a T helper lymphocyte marker, in the spleen was evaluated by immunofluorescence staining after CCl_4 treatment for 3 and 6 weeks. Original magnification ×40. **c** The CD4-positive area was quantified as a percentage using Image J. **d** Quantitative reverse transcription PCR was performed to measure messenger RNA (*mRNA*) expression levels of *Cd4* in the spleen. *Gapdh* was used as an internal control. **e** Splenic lymphocytes of the control and CCl_4 treatment group mice were analysed for CD4 expression by flow cytometry. The proportion of $CD4^+$ cells among total splenic cells is shown. The mean ± the standard deviation of values found in at least six mice is shown. $^*P < 0.05$, $^{**}P < 0.01$, $^{***}P < 0.001$

reduced to 4.49 ± 0.80 % and 3.18 ± 0.26 % after CCl_4 treatment for 3 and 6 weeks, respectively (3 weeks, $P = 0.0043$; 6 weeks, $P = 0.0040$; Fig. 5c). *Cd4* mRNA expression was also decreased by 0.75- and 0.58-fold after CCl_4 treatment for 3 and 6 weeks, respectively (3 weeks, $P = 0.030$; 6 weeks, $P = 0.0039$; Fig. 5d). The proportion

of $CD4^+$ lymphocytes to total splenic cells showed a time-dependent decrease after CCl_4 treatment (15.4 ± 0.67 % before CCl_4 treatment, 12.2 ± 1.39 % at 3 weeks after CCl_4 treatment, and 8.54 ± 2.65 % at 6 weeks after CCl_4 treatment; Fig. 5e). Similar findings were obtained in the TAA-induced liver injury model (Fig. S6).

The $CD4^+$ cells accumulated in the liver after toxin-induced liver injuries as demonstrated by the increase of the $CD4^+$ area and *Cd4* mRNA expression in the liver (Fig. S7). Splenectomy slightly reduced the accumulation of $CD4^+$ cells, although the difference did not reach statistical significant.

Splenic $CD4^+$ cells migrate to the liver in the CCl_4-induced liver injury model

The decrease in the number of T helper cells in the spleen prompted us to explore their fate after CCl_4-induced liver injury. For this purpose, we isolated splenic cells from C57BL/6-Tg mice ubiquitously expressing an enhanced green fluorescent protein (GFP) [19]. The GFP^+ splenic cells were transplanted into the spleen of syngeneic wild-type mice, and liver injury was induced by CCl_4. Livers were examined on the days following the injection of the first, third, and fifth doses of CCl_4. The migration of spleen-derived T helper cells in the liver was evaluated by GFP and CD4 immunostaining.

In the control groups, GFP^+ cells were scarcely seen in the liver, and they were almost negative for CD4 (Fig. S8a). In the CCl_4-induced liver injury model, we observed a time-dependent increase in the number of GFP^+ cells in the liver (Fig. 6a). Immunostaining for CD4 revealed that the $CD4^+$ cell count was also increased in a time-dependent manner (Fig. S8b). Furthermore, the number of GFP^+CD4^+ cells (spleen-derived T helper lymphocytes) was time-dependently increased (three doses, 6.9 ± 0.4/×100 high-power field, five doses, 11.1 ± 1.1/×100 high-power field). The proportion of GFP^+ cells among the $CD4^+$ cells in the liver was 24.5 ± 1.72 % and 22.4 ± 1.62 % after three and five injections of CCl_4, respectively (Fig. S8c). To exclude the possibility that circulating GFP^+ lymphocytes, not splenic GFP^+ lymphocytes, were the source of GFP^+ lymphocytes in the liver, we splenectomized mice 20 min after inoculation of the spleen with GFP^+ splenocytes, and determined whether GFP^+ lymphocytes appeared in the liver after fibrosis induction. Immunostaining showed that there were few GFP^+CD4^+ cells in the liver (Fig. 6a), indicating that the major source of GFP^+ lymphocytes appearing in the liver was not circulating GFP^+ lymphocytes.

GFP^+CD4^+ cells (spleen-derived T helper lymphocytes) in the liver were analysed for CD45RC expression by flow cytometry. The percentage of Th2 ($CD45RC^{low}$) lymphocytes was almost 100 % in GFP^+CD4^+ cells, whereas it was 88.0 ± 5.2 % in GFP^-CD4^+ cells, indicating that T helper lymphocytes migrating from the spleen were Th2 dominant compared with the resident T lymphocytes in the liver (Fig. 6b).

Fig. 6 T helper type 2 (*Th2*)-predominant spleen-derived T helper lymphocytes migrate from the spleen to the liver in response to liver injury. Splenic lymphocytes isolated from transgenic mice ubiquitously expressing green fluorescent protein (*GFP*) were transplanted into the spleens of syngeneic wild-type mice. Liver fibrosis was induced by injection of CCl_4. The mice were killed at 24 h after the first, third, and fifth injection. **a** Double immunofluorescence staining for GFP (*green*) and CD4 (*red*) with or without splenectomy. Original magnification ×100. **b** $CD4^+$ cells in the liver after the fifth injection were analysed for CD45RC expression to determine their T helper type 1 (*Th1*; ($CD45RC^{high}$) and Th2 ($CD45RC^{low}$) phenotype by flow cytometry. The relative proportion of Th1 and Th2 lymphocytes among intrahepatic GFP^+CD4^+ lymphocytes or GFP^-CD4^+ lymphocytes is shown. The mean ± the standard deviation of values obtained in seven mice is shown. *DAPI* 4′,6-diamidino-2-phenylindole

Transfer of splenocytes cancels the suppressive effect of splenectomy on liver fibrosis

The contribution of Th2-dominant splenic lymphocytes to liver fibrosis was investigated by adoptive transfer of isolated splenocytes to splenectomized mice. In this experiment, we evaluated liver fibrosis in the 3-week CCl_4 model (not the 6-week model) considering a short life span of injected splenic lymphocytes. Sirius red staining demonstrated that collagen deposition in the splenocyte-transferred CCl_4 splenectomy group was significantly enhanced compared with that in the PBS-injected CCl_4 splenectomy group, and it was comparable to that in the CCl_4 sham-operation group (Fig. 7a, b). The hydroxyproline content was also elevated in the splenocyte-transferred CCl_4 splenectomy group compared with the PBS-injected CCl_4 splenectomy group (282 ± 74.1 ng/mg vs 234 ± 13.5 ng/mg, $P = 0.026$; Fig. 7c). The expression level of *Col1a1* was enhanced in the splenocyte-transferred CCl_4 splenectomy group compared with the PBS-injected CCl_4 splenectomy group ($P = 0.026$; Fig. 7d). Hepatic expression of α-SMA was also enhanced in the splenocyte-transferred CCl_4 splenectomy group compared with the PBS-injected CCl_4 splenectomy group, as demonstrated by immunostaining (Fig. 7e) and qRT-PCR ($P = 0.030$; Fig. 7f). These results demonstrated that transfer of splenocytes cancelled the suppressive effect of splenectomy on liver fibrosis.

Discussion

This study demonstrates that splenectomy inhibited toxin-induced liver fibrosis in mice. A few experimental studies have shown that splenectomy suppressed liver fibrosis;

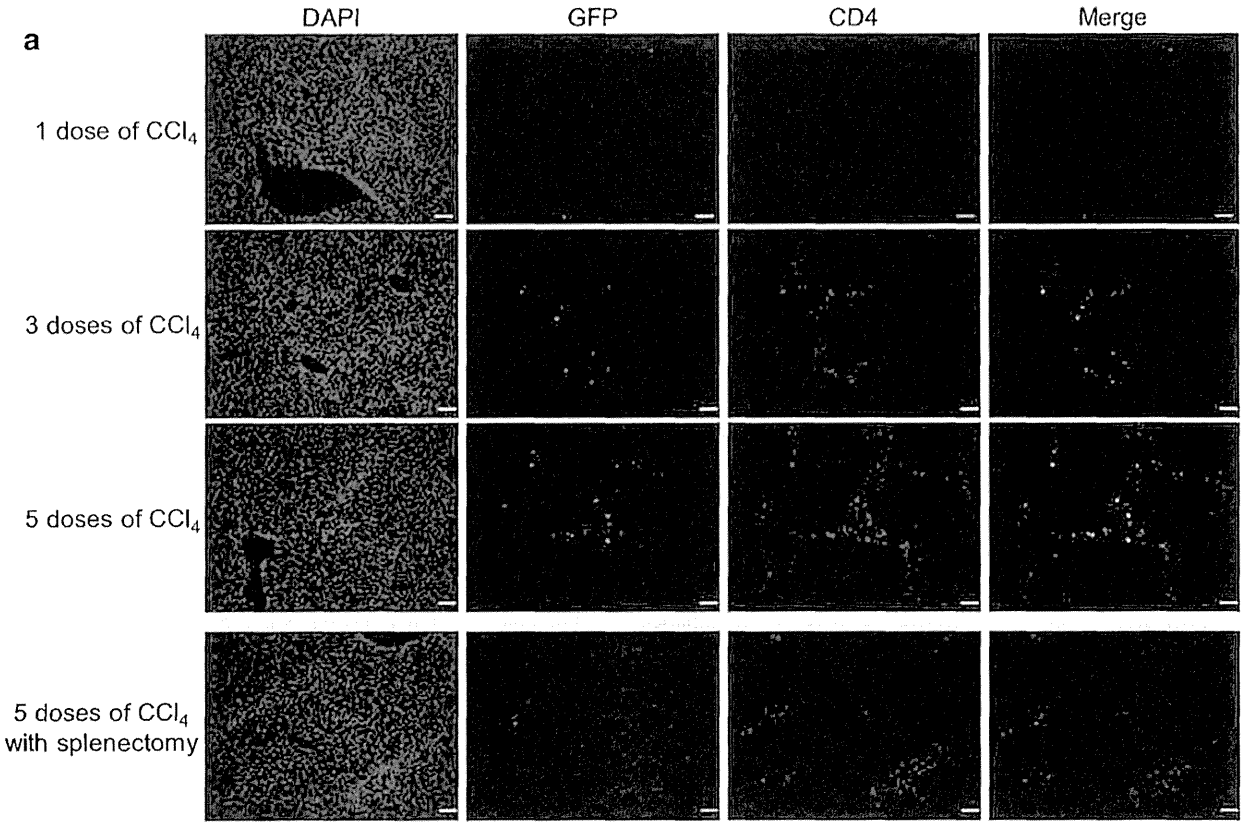
a
DAPI
GFP
CD4
Merge
1 dose of CCl_4
3 doses of CCl_4
5 doses of CCl_4
5 doses of CCl_4 with splenectomy

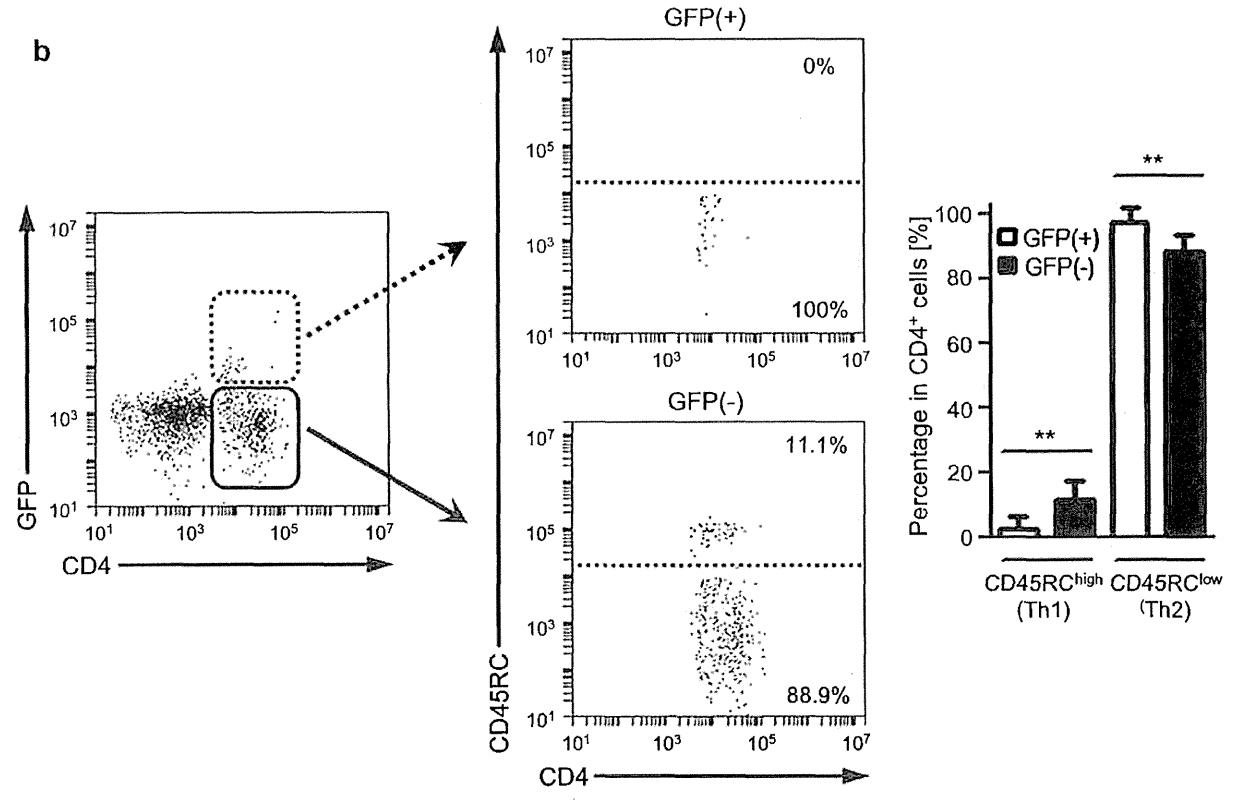
b
GFP
CD4
GFP(+)
0%
100%
GFP(-)
11.1%
88.9%
CD45RC
CD4
Percentage in CD4+ cells [%]
GFP(+)
GFP(-)
**
**
CD45RChigh (Th1)
CD45RClow (Th2)

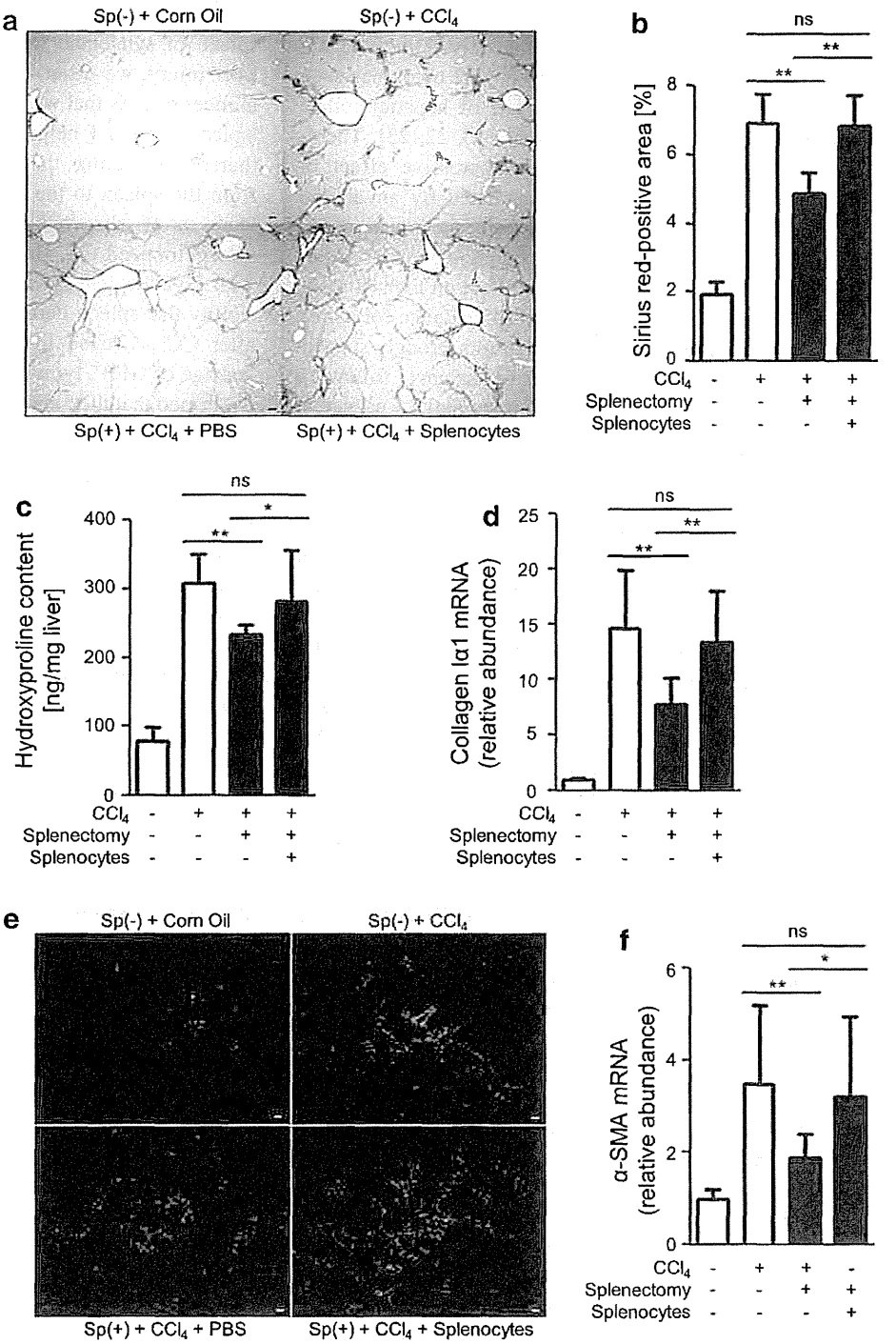

Fig. 7 Transfer of splenocytes cancels the suppressive effect of splenectomy on liver fibrosis. Liver fibrosis was induced by repetitive administration of CCl_4 after adoptive transfer of the isolated splenocytes or phosphate-buffered saline (*PBS*) as a control via the portal vein into syngeneic splenectomized mice. Liver fibrosis was evaluated after 3 weeks of CCl_4 treatment. **a** Liver fibrosis was evaluated by Sirius red staining. Original magnification ×40. **b** The Sirius red positive area was quantified as a percentage using Image J. **c** Collagen deposition was quantified by measuring the hydroxyproline content in the liver. **d** Quantitative reverse transcription PCR (qRT-PCR) was performed to measure messenger RNA (*mRNA*) expression levels of *Col1a1*. *Gapdh* was used as an internal control. **e** Activation of hepatic stellate cells was evaluated by immunofluorescence staining for α-smooth muscle actin (*α-SMA*). Original magnification ×40. **f** Hepatic expression levels of *Acta2* mRNA were measured using qRT-PCR. *Gapdh* was used as an internal control. The mean ± the standard deviation of values obtained in seven mice is shown. $*P < 0.05$, $**P < 0.01$, *ns* not significant, *Sp(-)* sham-operation group, *Sp(+)* splenectomy group

however, the mechanisms underlying this phenomenon are largely unknown [5–7]. In the present study, we focused on the immunological implication of the spleen. The spleen is a lymphoid organ where lymphocytes mature. In addition, the spleen is directly connected to the liver via the splenic and portal veins and is an important constituent of the portal system. Therefore, it is plausible that the spleen influences the immunological status of the liver.

In this study, splenectomy modified the balance of Th1/Th2 cytokine expression towards Th1 dominance in the liver in CCl_4-induced and TAA-induced liver fibrosis models. Previous studies have revealed that Th1 cytokines

have a suppressive effect on liver fibrosis. In particular, interferon-γ is a potent inhibitor of the activation of hepatic stellate cells [20, 21]. By comparison, Th2 cytokines such as IL-4 and IL-13 promote activation of hepatic stellate cells and progression of liver fibrosis [16, 22, 23]. Therefore, our results suggest that the suppressive effect of splenectomy on liver fibrosis is mediated by an altered Th1/Th2 balance. To verify our hypothesis, we used immunodeficient SCID mice lacking functional lymphocytes [24]. In SCID mice, the suppressive effect on liver fibrosis, as well as the influence on the Th1/Th2 balance following splenectomy, was abrogated. These results strongly suggest that the modified Th1/Th2 cytokine balance following splenectomy observed in wild-type mice plays a causative role in the inhibition of liver fibrosis.

Interestingly, SCID mice lacking profibrotic Th2 lymphocytes showed liver fibrosis in response to CCl_4 to the same extent as or to an even higher extent than immunocompetent wild-type mice. Although the significance of lymphocyte proinflammatory and profibrotic properties has been well recognized, recent studies have demonstrated that there are lymphocyte subsets that regulate and control inflammatory response, such as regulatory T cells or $\gamma\delta$ T cells. For example, deficiency in regulatory T cells aggravates the progression of liver fibrosis [25]. We suppose that the lack of an immunomodulatory response by these lymphocytes in SCID mice might have contributed to enhancement of the fibrogenic response, although this is only speculation and needs to be investigated further.

Previous studies have implied other antifibrotic mechanisms mediated by splenectomy. For instance, it was suggested that platelets themselves could inhibit the development of liver fibrosis and that splenectomy exerted an antifibrotic effect via thrombocytosis [5, 6]. Comparatively, Akahoshi et al. [7] proposed that the loss of spleen-derived transforming growth factor β_1 mediated the inhibitory effect of splenectomy on liver fibrosis. Decreases in portal flow and portal pressure are other possible mechanisms of the antifibrotic effect of splenectomy. Although our study did not preclude the aforementioned mechanisms, our observation that the splenectomy-mediated antifibrotic effect was abrogated in SCID mice strongly supports the proposal that immunological mechanisms are involved in this phenomenon.

We explored the mechanisms by which splenectomy modifies the Th1/Th2 balance in the liver. We observed that the number of $CD4^+$ cells (T helper lymphocytes) in the spleen was dramatically decreased after liver injury. In contrast, the number of $CD4^+$ cells was increased in the liver. These observations led us to speculate that T helper lymphocytes in the spleen migrated to the liver in response to liver injury. To examine our hypothesis, we isolated GFP^+ splenic cells from C57BL/6-Tg(CAG-EGFP)C14-Y01-FM131Osb mice and transplanted them into the spleen of syngeneic wild-type mice. After CCl_4-induced liver injury, we observed time-dependent increases in the number of cells that were double positive for GFP and CD4 (spleen-derived T helper lymphocytes) in the injured liver, thereby indicating that T helper lymphocytes migrated from the spleen to the liver. GFP^+ T helper lymphocytes were rarely observed in the control (corn oil) mice or splenectomized CCl_4-induced liver injury mice inoculated with GFP^+ splenocytes. These results precluded the possibility that spleen-derived T helper lymphocytes observed after CCl_4-induced liver injury were merely due to the leakage of GFP^+ lymphocytes at the time of injection, and confirmed that they migrated from the spleen in response to liver injury. Swirski et al. [26] reported that splenic monocytes migrated to the injured site in response to ischaemic myocardial injury, and discovered a novel role of the spleen as a site for storage and rapid deployment of monocytes. Similarly to their findings, the present study demonstrates that the spleen functions as a site for storage and mobilization of T helper lymphocytes in response to liver injury.

Th2 lymphocytes are the main constituent of the immune environment in the spleen [27, 28]. Furthermore, in this study, we observed that most of the spleen-derived T helper cells in the liver were Th2 lymphocytes after liver injury. From our findings taken together, we propose that following liver injury, Th2-predominant splenic T lymphocytes migrate to the liver and promote liver fibrosis by modifying the Th1/Th2 balance in the liver towards Th2 dominance. Splenectomy decreases the absolute number of Th2 lymphocytes in the liver and reverses this Th1/Th2 imbalance, resulting in inhibition of liver fibrosis.

The origin of Th1 lymphocytes on liver injuries is another important issue. Lymphoid organs other than the spleen, such as marrow and thymus, may be possible sources of Th1 lymphocytes, although this is speculation. Further studies are needed to elucidate this.

Comparatively, splenectomy did not influence the progression of liver fibrosis and the liver Th1/Th2 cytokine balance in the BDL-induced liver injury model. The reason for the discrepancy between toxin-induced and cholestasis-induced liver injury models is of interest. Clinical observations have shown that the immune function is disturbed in patients with obstructive jaundice. For instance, inhibition of cellular immunity and suppression of the T lymphocyte proliferative response in jaundice were suggested [29, 30]. Animal studies have also shown that obstructive jaundice strongly influences the immune status. Katz et al. [31] demonstrated that obstructive jaundice expanded the number of regulatory T lymphocytes, which in turn suppressed bulk T cell functions in the liver. In addition, other studies have shown that BDL influenced splenocyte

activity such as mitogenic response [32]. Thus, we speculate that the functional suppression of T helper cells in the liver and/or the selective depression of the lymphocytes derived from the spleen in obstructive jaundice may be the reasons why the effect of splenectomy on the development of liver fibrosis and the Th1/Th2 balance in the liver was not seen in the BDL model. However, further studies are needed to investigate this hypothesis.

In conclusion, the present study unveiled a novel role of the spleen in the progression of liver fibrosis as a site for storage and mobilization of T helper lymphocytes in response to liver injury. Further clinical studies are required to verify the beneficial effect of splenectomy on liver fibrosis in clinical situations. Our findings provide new insights into the use of immunomodulation as an effective strategy for treatment of liver fibrosis. This conclusion might be particularly important in the setting of liver transplantation to treat hepatitis C, as various immunosuppressive regimens may affect the progression of liver fibrosis differently, if the eradication of the virus is unsuccessful. A more detailed understanding of the mechanisms underlying these observations may allow the development of clinically useful immunosuppressive regimens.

Acknowledgment This work was supported by a grant from the Japan Society for the Promotion of Science: Grant-in-Aid for Scientific Research (B), no. 23390322.

Conflict of interest The authors declare that they have no conflict of interest.

References

1. Friedman SL. Mechanisms of hepatic fibrogenesis. Gastroenterology. 2008;134:1655–69.
2. Murata K, Ito K, Yoneda K, et al. Splenectomy improves liver function in patients with liver cirrhosis. Hepatogastroenterology. 2008;55:1407–11.
3. Imura S, Shimada M, Utsunomiya T, et al. Impact of splenectomy in patients with liver cirrhosis: results from 18 patients in a single center experience. Hepatol Res. 2010;40:894–900.
4. Sugawara Y, Yamamoto J, Shimada K, et al. Splenectomy in patients with hepatocellular carcinoma and hypersplenism. J Am Coll Surg. 2000;190:446–50.
5. Watanabe M, Murata S, Hashimoto I, et al. Platelets contribute to the reduction of liver fibrosis in mice. J Gastroenterol Hepatol. 2009;24:78–89.
6. Kodama T, Takehara T, Hikita H, et al. Thrombocytopenia exacerbates cholestasis-induced liver fibrosis in mice. Gastroenterology. 2010;138:2487–98.
7. Akahoshi T, Hashizume M, Tanoue K, et al. Role of the spleen in liver fibrosis in rats may be mediated by transforming growth factor β-1. J Gastroenterol Hepatol. 2002;17:59–65.
8. Shi Z, Wakil AE, Rockey DC. Strain-specific differences in mouse hepatic wound healing are mediated by divergent T helper cytokine responses. Proc Natl Acad Sci U S A. 1997;30(94):10663–8.
9. Patsenker E, Schneider V, Ledermann M, et al. Potent antifibrotic activity of mTOR inhibitors sirolimus and everolimus but not of cyclosporine A and tacrolimus in experimental liver fibrosis. J Hepatol. 2011;55:388–98.
10. van der Laan LJ, Hudson M, McPherson S, et al. Results of a two-center study comparing hepatic fibrosis progression in HCV-positive liver transplant patients receiving cyclosporine or tacrolimus. Transplant Proc. 2010;42:4573–7.
11. Taura K, Miura K, Iwaisako K, et al. Hepatocytes do not undergo epithelial-mesenchymal transition in liver fibrosis in mice. Hepatology. 2010;51:1027–36.
12. Popov Y, Sverdlov DY, Sharma AK, et al. Tissue transglutaminase does not affect fibrotic matrix stability or regression of liver fibrosis in mice. Gastroenterology. 2011;140:1642–52.
13. Taura K, De Minicis S, Seki E, et al. Hepatic stellate cells secrete angiopoietin 1 that induces angiogenesis in liver fibrosis. Gastroenterology. 2008;135:1729–38.
14. Arias-Diaz J, Ildefonso JA, Muñoz JJ, et al. Both tacrolimus and sirolimus decrease Th1/Th2 ratio, and increase regulatory T lymphocytes in the liver after ischemia/reperfusion. Lab Investig. 2009;89:433–5.
15. Novobrantseva TI, Majeau GR, Amatucci A, et al. Attenuated liver fibrosis in the absence of B cells. J Clin Investig. 2005;115:3072–82.
16. Farah IO, Mola PW, Kariuki TM, et al. Repeated exposure induces periportal fibrosis in Schistosoma mansoni-infected baboons: role of TGF-β and IL-4. J Immunol. 2000;164:5337–43.
17. Subra JF, Cautain B, Xystrakis E, et al. The balance between $CD45RC^{high}$ and $CD45RC^{low}$ CD4 T cells in rats is intrinsic to bone marrow-derived cells and is genetically controlled. J Immunol. 2001;166:2944–52.
18. Nishimura H, Hattori S, Abe M, et al. Differential expression of three CD45 alternative structures on murine T cells: exon 6-dependent epitope as a marker for functional heterogeneity of CD4+ T cells. Int Immunol. 1992;4:923–30.
19. Okabe M, Ikawa M, Kominami K, et al. 'Green mice' as a source of ubiquitous green cells. FEBS Lett. 1997;407:313–9.
20. Czaja MJ, Weiner FR, Takahashi S, et al. γ-Interferon treatment inhibits collagen deposition in murine schistosomiasis. Hepatology. 1989;10:795–800.
21. Baroni GS, D'Ambrosio L, Curto P, et al. Interferon gamma decreases hepatic stellate cell activation and extracellular matrix deposition in rat liver fibrosis. Hepatology. 1996;23:1189–99.
22. Wynn TA. Fibrotic disease and the T_H1/T_H2 paradigm. Nat Rev Immunol. 2004;4:583–94.
23. Cheever AW, Williams ME, Wynn TA, et al. Anti-IL-4 treatment of Schistosoma mansoni-infected mice inhibits development of T cells and non-B, non-T cells expressing Th2 cytokines while decreasing egg-induced hepatic fibrosis. J Immunol. 1994;153:753–9.
24. Bosma GC, Custer RP, Bosma MJ. A severe combined immunodeficiency mutation in the mouse. Nature. 1983;301:527–30.
25. Roh YS, Park S, Lim CW, et al. Depletion of Foxp3+ regulatory T cells promotes profibrogenic milieu of cholestasis-induced liver injury. Dig Dis Sci. 2014. doi:10.1007/s10620-014-3438-2.
26. Swirski FK, Nahrendorf M, Etzrodt M, et al. Identification of splenic reservoir monocytes and their deployment to inflammatory sites. Science. 2009;325:612–6.
27. Vitetta ES, Brooks K, Chen YW, et al. T-cell-derived lymphokines that induce IgM and IgG secretion in activated murine B cells. Immunol Rev. 1984;78:137–57.
28. Coffman RL, Seymour BW, Lebman DA, et al. The role of helper T cell products in mouse B cell differentiation and isotype regulation. Immunol Rev. 1988;102:5–28.

29. Vierucci A, De Martino M, Novembre E, et al. Effect of the serum of patients with cholestasis on lymphocyte E rosette formation. Ann Sclavo. 1977;19:1119–29.
30. Li H, Xiong ST, Zhang SX, et al. Interleukin 2 production and its relationship with T lymphocyte subsets in patients with obstructive jaundice. J Tongji Med Univ. 1992;12:164–8.
31. Katz SC, Ryan K, Ahmed N, et al. Obstructive jaundice expands intrahepatic regulatory T cells, which impair liver T lymphocyte function but modulate liver cholestasis and fibrosis. J Immunol. 2011;187:1150–6.
32. Chaignaud BE, White JG, Nie CH, et al. Splenocytes from bile duct ligated rats do not elicit a normal immune response in the intact host. Am Surg. 1994;60:7–11.

Hindawi Publishing Corporation
BioMed Research International
Article ID 387653

Hindawi

Research Article

Evaluation of Liver Fibrosis Using Texture Analysis on Combined-Contrast-Enhanced Magnetic Resonance Images at 3.0T

Takeshi Yokoo,[1,2] Tanya Wolfson,[3] Keiko Iwaisako,[1,4,5] Michael R. Peterson,[6] Haresh Mani,[7] Zachary Goodman,[8] Christopher Changchien,[1] Michael S. Middleton,[1] Anthony C. Gamst,[3] Sameer M. Mazhar,[4] Yuko Kono,[1] Samuel B. Ho,[4,9] and Claude B. Sirlin[1]

[1]*Departments of Radiology, University of California, San Diego, CA 92103, USA*
[2]*Department of Radiology and Advanced Imaging Research Center, University of Texas Southwestern Medical Center, 2201 Inwood Road, NE2.210B, Dallas, TX 75390-9085, USA*
[3]*Computational and Applied Statistics Laboratory, San Diego Supercomputer Center, University of California, San Diego, CA 92093, USA*
[4]*Departments of Medicine, University of California, San Diego, CA 92103, USA*
[5]*Department of Target Therapy Oncology, Kyoto University Graduate School of Medicine, Kyoto, Japan*
[6]*Departments of Pathology, University of California, San Diego, CA 92103, USA*
[7]*Department of Pathology, Penn State Hershey Medical Center, Hershey, PA 17033, USA*
[8]*Center for Liver Diseases, Inova Fairfax Hospital, Falls Church, VA 22042, USA*
[9]*VA San Diego Healthcare System, San Diego, CA 92161, USA*

Correspondence should be addressed to Takeshi Yokoo; takeshi.yokoo@utsouthwestern.edu

Received 29 July 2014; Revised 15 October 2014; Accepted 18 October 2014

Academic Editor: Trevor Andrews

Purpose. To noninvasively assess liver fibrosis using combined-contrast-enhanced (CCE) magnetic resonance imaging (MRI) and texture analysis. *Materials and Methods.* In this IRB-approved, HIPAA-compliant prospective study, 46 adults with newly diagnosed HCV infection and recent liver biopsy underwent CCE liver MRI following intravenous administration of superparamagnetic iron oxides (ferumoxides) and gadolinium DTPA (gadopentetate dimeglumine). The image texture of the liver was quantified in regions-of-interest by calculating 165 texture features. Liver biopsy specimens were stained with Masson trichrome and assessed qualitatively (METAVIR fibrosis score) and quantitatively (% collagen stained area). Using L_1 regularization path algorithm, two texture-based multivariate linear models were constructed, one for quantitative and the other for quantitative histology prediction. The prediction performance of each model was assessed using receiver operating characteristics (ROC) and correlation analyses. *Results.* The texture-based predicted fibrosis score significantly correlated with qualitative ($r = 0.698$, $P < 0.001$) and quantitative ($r = 0.757$, $P < 0.001$) histology. The prediction model for qualitative histology had 0.814–0.976 areas under the curve (AUC), 0.659–1.000 sensitivity, 0.778–0.930 specificity, and 0.674–0.935 accuracy, depending on the binary classification threshold. The prediction model for quantitative histology had 0.742–0.950 AUC, 0.688–1.000 sensitivity, 0.679–0.857 specificity, and 0.696–0.848 accuracy, depending on the binary classification threshold. *Conclusion.* CCE MRI and texture analysis may permit noninvasive assessment of liver fibrosis.

1. Introduction

The ongoing epidemic of Chronic Liver Disease (CLD) is a major contributor to liver-related mortality and morbidity in the United States. More than 20,000 Americans die from CLD complications each year [1]. The most common etiologies for CLD are chronic hepatitis C virus (HCV) infection and alcoholic hepatitis [2, 3]. Over 4 million Americans are HCV

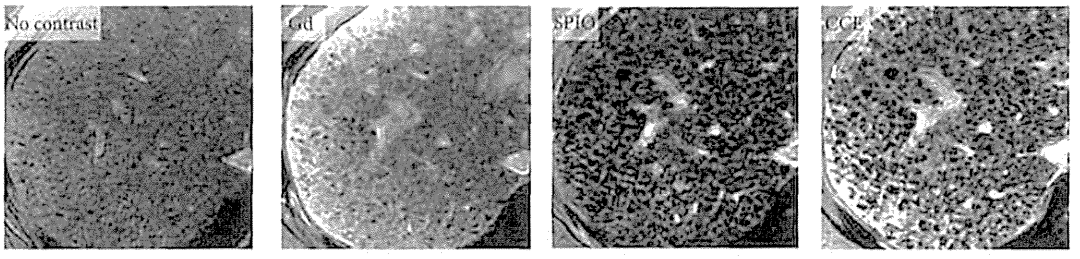

FIGURE 1: MR images of liver in 60-year old man with HCV-related cirrhosis. Noncontrast, Gd-only, SPIO-only, and CCE 2D breath-hold T1-weighted gradient-echo images of cirrhotic liver due to HCV. Abnormal reticular pattern of the liver parenchyma is better visualized on single-contrast-enhanced (Gd or SPIO) images than on unenhanced image and better visualized on CCE images than on single-contrast-enhanced images. Gd: gadolinium; SPIO: superparamagnetic iron oxide, and CCE: combined contrast enhanced.

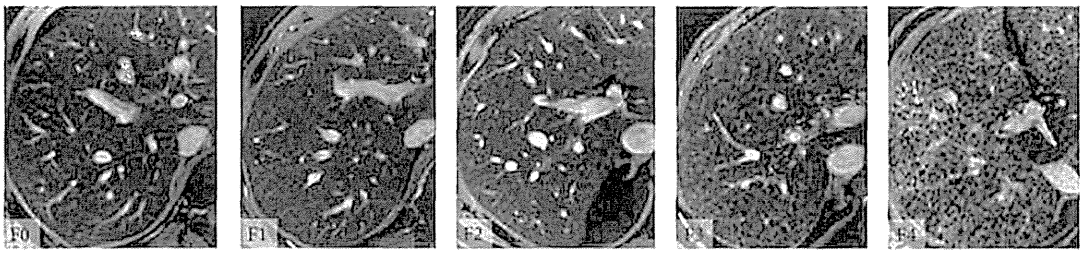

FIGURE 2: Combined contrast enhanced (CCE) MR images at various stages of fibrosis. CCE MR images in adults with chronic HCV infection and histologically determined Metavir fibrosis stages F0, F1, F2, F3, and F4. Subjectively, the reticular texture of the liver parenchyma becomes progressively more pronounced with increasing Metavir fibrosis stage.

carriers, but many are asymptomatic and unaware of their infection [4].

The common pathway in the natural history of CLD, including chronic HCV infection, is progressive liver fibrosis and ultimately cirrhosis [5]. Fibrosis indicates cumulative liver damage, contributes to the development of portal hypertension and hepatic dysfunction, and predicts poor clinical outcome [6, 7]. Most liver-related mortality and morbidity occur in the cirrhotic population [8]. Assessment of liver fibrosis is therefore critical in the management of patients with CLD.

The current gold standard for fibrosis evaluation is liver biopsy. The severity of fibrosis due to HCV infection is often classified using an ordinal scale such as the Metavir system [9]. However, biopsy is invasive and thus problematic for frequent monitoring. Moreover, its interpretation is subjective, leading to inter- and intraobserver variability [10–12]. For these reasons, noninvasive and objective techniques are under investigation, including fibrosis-specific serum markers [13, 14], ultrasound elastography [15, 16], magnetic resonance (MR) elastography [17–19], diffusion weighted MR imaging [20–22], and single-contrast-enhanced MR imaging [23–25].

Another promising MR imaging-based technique is combined-contrast-enhanced (CCE) MR imaging [26]. This technique exploits the complementary effects of positive contrast enhancement by gadolinium-chelates (Gd) and negative enhancement by superparamagnetic iron oxide (SPIO) agents. Compared to noncontrast, Gd-enhanced, or SPIO-enhanced images, CCE images better depict the reticular signal abnormalities associated with fibrosis as shown in Figure 1 [27]. The conspicuity of this pattern appears to parallel histologic fibrosis severity (Figure 2) suggesting that liver fibrosis can be assessed by the severity of the "texture" abnormality.

The potential role of texture analysis in liver fibrosis assessment was previously explored in retrospective studies using qualitative [26] and quantitative [26, 28–30] texture analysis. The purpose of this prospective study was to provide proof-of-concept that quantitative texture analysis using CCE MR imaging may permit noninvasively assess liver fibrosis in adults with HCV infection using CCE MR imaging.

2. Method and Materials

2.1. Study Design and Subjects. This prospective, cross-sectional, observational clinical study was approved by an institutional review board and is HIPAA-compliant. Potential eligible subjects were referred for research MR imaging examination from hepatology clinics at our institution. Written informed consents were obtained. Selection criteria are listed in Table 1. Patient recruitment was stratified according to the fibrosis severity at liver biopsy and continued until at least five subjects in each fibrosis severity category (per clinical biopsy reports) were enrolled.

2.2. Liver Biopsy. Subjects had a percutaneous 16-gauge needle-core biopsy of the right hepatic lobe for clinical care by the referring hepatologists. Specimens were processed in

Table 1: Selection criteria.

Inclusion criteria	Exclusion criteria
(i) Age >18 years (ii) Newly diagnosed HCV infection, without clinically overt cirrhosis (iii) Recent or planned biopsy[1] (iv) Willing and able to undergo CCE MRI exam within 30 days of biopsy (v) Willing and able to undergo phlebotomy for estimated GFR determination within 30 days of biopsy	(i) Estimated GFR <60 mL/mL ($N = 0$ potential subjects) (ii) Imaging not performed within 30 days of biopsy ($N = 2$) (iii) Nondiagnostic biopsy or trichrome slide unavailable ($N = 2$) (iv) Contraindication to MR exam ($N = 1$)[2] (v) Lack of intravenous access ($N = 1$) (vi) History of severe allergic reaction or anaphylaxis ($N = 0$) (vii) History of liver diseases other than HCV including iron overload ($N = 0$) (viii) Severe claustrophobia ($N = 0$) (ix) Pregnant or nursing mother ($N = 0$)

[1]Biopsies were performed for clinical care. [2]Due to intraorbital shrapnel. GFR: glomerular filtration rate. Parenthesis () contains the number of potential subjects excluded for the criterion.

the pathology department per routine protocol, including Masson-trichrome staining. Clinical biopsy reports were generated by staff pathologists. Each clinical report included assessment of fibrosis severity (none, mild, moderate, severe, and cirrhosis); the clinically reported fibrosis severity was used for the block recruitment but not analyzed.

2.3. Qualitative and Quantitative Scoring of Histology. The trichrome-stained slides were further evaluated for research purposes. The entire slides were digitized using an APERIO ScanScope scanner (Aperio Technologies, Inc., Vista, CA). The digitized images were viewed using the Aperio ImageScope software and the fibrosis severity was scored qualitatively by histomorphology and quantitatively by digital image analysis.

Qualitative scoring was performed independently by three pathologists with expertise in liver pathology (MRP, HM, and ZG). Without knowledge of clinical, MR imaging, or quantitative histology findings, each reader reviewed the digitized histology images, subjectively assessed the adequacy of each specimen, and assigned to each specimen a Metavir fibrosis score, F0–F4. The readers were blinded to each other's scores. Other histology features (e.g., necro-inflammation, steatosis, iron) were not recorded. To assess adequacy of specimen, one pathologist (MRP) counted the number of portal triads within each noncirrhotic specimen; portal triads were not counted in cirrhotic specimens due to architectural distortion. The total length of each specimen was recorded.

Quantitative scoring was performed by a hepatology research scientist (KI) using ImageScope software analysis tools, without knowledge of the clinical, MR imaging, or qualitative histology findings. Staining variability was corrected by digitally adjusting color saturation. Total specimen area was manually segmented, and the blue-stained pixels (representing collagen) were segmented using manual intensity thresholding. Percent (%) collagen was calculated as the ratio of blue-stained to total specimen pixels.

2.4. MR Imaging. Subjects received SPIO (ferumoxides, Feridex, Bayer HealthCare Pharmaceuticals, Wayne, NJ) continuous intravenous infusion (0.5 mL/kg) diluted in 100 mL of 5% dextrose solution, passed through a 5-μm filter at 2–4 mL/min over 30 minutes per manufacturer's instructions. Thirty minutes after completion of SPIO infusion, subjects were scanned supine in a superconducting MR whole body system at 3T (GE Signa EXCITE HD, GE Medical Systems, Milwaukee, WI), with an 8-channel torso phase-array coil and a dielectric pad centered over the liver. Gadolinium-DTPA (gadopentetate dimeglumine, Magnevist, Bayer HealthCare Pharmaceuticals, Wayne, NJ) was injected intravenously (0.1 mmol/kg). Using a 2D chemically fat-saturated fast spoiled gradient-recalled echo (FSPGR) sequence without parallel imaging, four sets of axial CCE images of the liver were acquired during separate 18–28 second breath-holds, 4–10 minutes after Gd injection. In this 6-minute window, enhancement of the liver by the two agents (SPIO and Gd) is subjectively constant according to our clinical experience of CCE MR imaging in cirrhotic and noncirrhotic livers; moreover, the T1- and T2* shortening effects of gadopentetate and ferumoxides in liver may be assumed stable over this period from the known liver clearance rates of these agents [31–33]. The four image sets were acquired to help ensure that at least one set was free of visible motion artifacts. Imaging parameters included TR 100 ms, TE 6 ms, FA 70°, slice thickness 4 mm, interslice gap 4 mm, number of slices 5, and bandwidth 130 Hz/pixel. Two of the four image sets were acquired with 384 × 224 and two with 384 × 256 matrix. Field-of-view was adjusted to accommodate body habitus and breath-hold capacity. These parameters were selected to provide simultaneous T1- and T2*-weighting to exploit Gd- and SPIO-enhancement, respectively; adequate signal-to-noise ratio; high spatial resolution; and relatively short acquisition time. The Food and Drug Administration (IND number 75,579) approved off-label use of Magnevist-Feridex combined contrast for this research study.

2.5. Image Processing and Texture Analysis. A radiology resident (TY) and a trained research assistant (CC) analyzed the CCE images without knowledge of clinical or biopsy findings. From the four CCE image sets, the set with the highest resolution and subjectively least motion artifact was selected. Representative CCE images of the liver (1–5 sections per subject) were exported in DICOM format. Using MATLAB (Mathworks, Natick, MA), a total of five nonoverlapping rectangular regions-of-interest (ROIs) of size >100 mm^2 were placed per subject within areas of subjectively uniform texture

in the right hepatic lobe (Couinaud segments IV–VIII), avoiding artifacts, bile ducts, and vessels. Each ROI image was standardized by rotating to the Cartesian coordinate system with zero tilt-angle, interpolating to 0.5 mm/pixel resolution, removing bilinear spatial trend of signal intensities, and scaling to 0-1 intensity range.

Gradient and Laplacian transformations (1st and 2nd spatial derivatives) were applied to each standardized ROI to generate additional "edge-enhanced" and "zero-crossing" texture patterns. For each untransformed (original) and transformed (gradient, Laplacian) ROI, 55 texture features were calculated as detailed in the supplementary materials available online at http://dx.doi.org/10.1155/2014/387653. These texture features represented five texture feature classes: pixel intensity histogram, Gaussian mixture model, autocorrelation, cooccurrence matrices, and Voronoi polygons. These classes were selected based on the expected imaging characteristics of fibrosis texture, as explained in the supplementary materials. For each subject, the texture features were averaged across the five ROI's to generate a set of 165 average texture features.

2.6. Statistical Analyses

2.6.1. Comparison of Histologic Scores. For each subject, the average, standard deviation (STD), and range of the Metavir scores of the three pathology readers were calculated. The interreader agreement was assessed by intraclass correlation coefficient (ICC, two-way analysis for precise agreement) and their 95% confidence intervals (CIs) were calculated. ICC was also calculated for each pair of readers. The average Metavir scores of the three readers were compared to %-collagen scores using Pearson correlation analysis.

2.6.2. Comparison of Texture and Histology. A biostatistician (TW) performed statistical analysis using the 165 texture features to predict qualitative (Metavir) and quantitative (%-collagen) fibrosis scores. A path-following algorithm for L_1 regularized linear model called GLM-path [34] with a Gaussian link (i.e., linear regression) was used to identify the optimal linear model of texture features that minimized the fibrosis prediction error for each number of predictors (i.e., features). The optimal number of predictors was determined by Akaike Information Criterion (AIC) [35]. Using the qualitative and quantitative fibrosis scores as the reference, two texture-based fibrosis prediction models were constructed, respectively. For each subject, the predicted qualitative (Metavir) and quantitative (%-collagen) fibrosis scores were calculated using respective prediction models.

Pearson's correlation was used to evaluate the strength of the relationship between the predicted and histologic scores. Additionally, the performance of each prediction model for dichotomized classification was assessed using receiver-operating-characteristics (ROC) analysis using the average histologically determined Metavir score as the reference standard. At each of four classification thresholds (Metavir F1, F2, F3, and F4 for qualitative scoring; 5, 10, 15, and 20% collagen for quantitative scoring), the classification accuracy, sensitivity, and specificity (and their CIs) were calculated at the predicted fibrosis score cutoff value that maximized the sum of sensitivity and specificity.

The regularization employed by the GLM-path algorithm is designed to minimize prediction error over independent validation datasets [34]. Therefore no dedicated validation procedure was performed in this proof-of-concept study. However, the algorithm may not necessarily minimize the prediction error of the test dataset itself; thus, some degree of mismatch between the predicted and actual fibrosis scores is expected.

3. Results

3.1. Subjects. Between August 2007 and March 2009, 52 newly diagnosed HCV-positive adults (age 51.2 ± 6.3 years, 38 male, 12 female) with recent or planned liver biopsy were recruited for CCE imaging. Six subjects were excluded (Table 1). The remaining 46 subjects formed the study group. All subjects completed the MR examination without serious adverse effects. At least one CCE image set was subjectively adequate in quality for further image analyses in each subject.

3.2. Qualitative versus Quantitative Histology. Examples of biopsy specimens are shown in Figure 3. The histology specimen's average ± STD [range] of the total length and the number of portal triads were 21.9 ± 9.8 mm [6.7–44.2] and 14.2 ± 6.0 [4–28], respectively.

Figure 4(a) shows the histogram of qualitative Metavir scores assigned by the three readers. The 3-reader agreement was good with ICC of 0.772 (95% CI [0.653–0.859]). Pairwise ICCs were 0.727, 0.768, and 0.831, depending on the reader pairs. All readers agreed that all biopsy specimens were adequate.

Figure 4(b) shows the histogram of quantitative %-collagen rounded to the nearest 5%. Over half the subjects had rounded %-collagen ≤5%. As shown in Figure 5 the relationship between the qualitative (average Metavir) and quantitative (%-collagen) scores was curvilinear, as has been observed by others [36, 37]. Log-linear plot of quantitative (y-axis) and qualitative (x-axis) scores demonstrated significant linear correlation with Pearson's $r = 0.81$ ($P < 0.001$).

3.3. Image Texture versus Histology. The liver image textures of representative subjects are shown in Figure 6 with their respective qualitative (Metavir) and quantitative (%-collagen) scores.

Using qualitative histology as the reference, GLM-path analysis identified a set of 6 texture features predictive of Metavir fibrosis scores (Table 2). As shown in Figure 7(a), the Metavir score predicted by a 6-feature model linearly correlated with the average Metavir scores of the three readers with $r = 0.698$ ($P < 0.001$). Table 3 summarizes the ROC analysis results at each classification threshold. AUCs were 0.814–0.976, sensitivities 0.659–1.000, specificities 0.778–0.930, and accuracies 0.674–0.935, depending on the classification threshold.

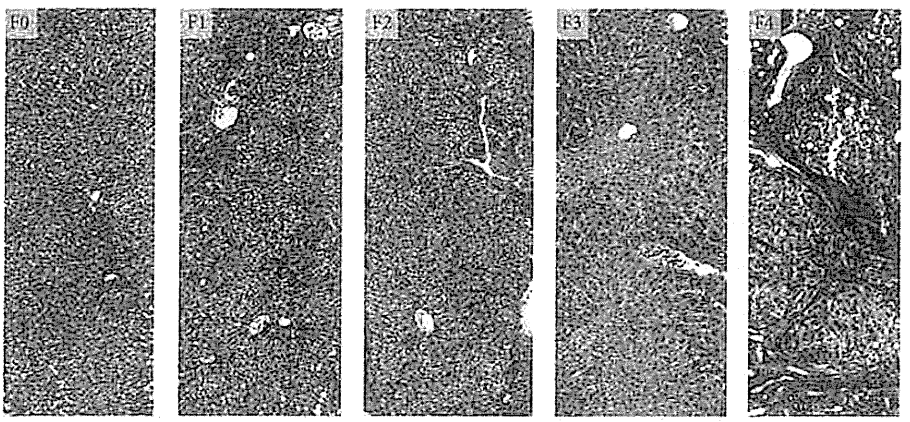

FIGURE 3: Histologic assessment of liver HCV-related fibrosis. Liver biopsy specimen from subjects with chronic HCV infection, stained with Masson-trichrome. F0 (absent fibrosis), F1 (stellate enlargement of portal tracts), F2 (enlarged portal tracts with rare septa), F3 (numerous septa without cirrhosis), and F4 (cirrhosis) according to Metavir scoring system. Trichrome stains fibrosis blue.

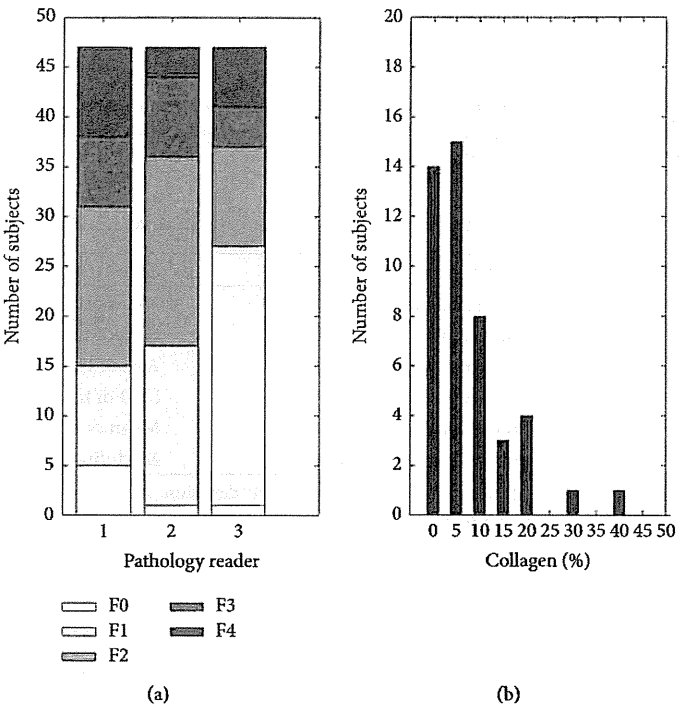

FIGURE 4: Fibrosis severity distribution. The study group's histograms by Metavir fibrosis score (left) and %-collagen (right). The most common Metavir fibrosis score was F1 or F2 depending on the reader. Nine subjects (19%; 9/46) had a score of F4 (cirrhosis) from at least one reader. %-collagen is rounded to the nearest 5%.

Using quantitative histology as the reference, GLM-path analysis identified another set of 6 texture features predictive of %-collagen scores (Table 4). As shown in Figure 5 (LEFT) the %-collagen score predicted by the 6-feature model linearly correlated with %-collagen score of histology with $r = 0.757$ ($P < 0.001$). Table 5 summarizes the ROC analysis results at threshold values at 5, 20, 15, and 20% fibrosis. AUCs were 0.742–0.950, sensitivities 0.688–1.000, specificities 0.679–0.857, and accuracies 0.696–0.848, depending on the classification threshold.

Identified texture features were similar but not identical between qualitative and quantitative prediction models (Tables 2 and 4). Two classes of texture features were common to both Gaussian-mixture model and Voronoi polygons. One class of texture features (pixel intensity histogram) was predictive only for qualitative scores. Texture features of both untransformed and transformed ROI images were found to be predictive. For illustration purposes, these texture classes derived from a ROI in a cirrhotic subject are shown in Figure 8.